Nanochem Res 4(2): 119-131, Summer and Autumn 2019

RESEARCH PAPER

The Stage Dependent Effect of Capping Agent Introduction in the Synthesis of Magnetite Nanoparticles

Matthew V. Hickson*, Zenixole R. Tshentu and Richard Betz

Department of Chemistry, Nelson Mandela University, Port Elizabeth, 6031, South Africa

ARTICLE INFO

Article History:
Received 25 April 2018
Accepted 13 August 2019
Published 15 October 2019

Keywords:
Amino Acids
Capping Agent
Magnetite Nanoparticles

ABSTRACT

In this paper, three techniques to obtain capped magnetite nanoparticles were compared. In the formation of magnetite nanoparticles via the co-precipitation route, capping agents were introduced pre-, simultaneously with, or post-addition of the precipitating agent, ammonia. The amino acids L-glutamine and L-glutamic acid were used as the capping agents. Characterization via TEM, PXRD, EDX, and magnetic analysis displayed that the stage of introduction affected the properties of the nanoparticles obtained. Confirmation of capping was performed by FTIR and X-ray photoelectron spectroscopy. TEM displayed that the post-addition method yielded nanoparticles with the narrowest size distributions, having attractive dispersity values. The pre- and simultaneously-introduced methods produced smaller nanoparticles but had relatively higher size distributions. Crystallite size determined from pXRD showed that the post-addition method had the highest crystallite size, even compared to the uncapped nanoparticles, while the pre-introduced were much less crystalline. From the magnetic studies, the post-introduction method was shown to yield the highest magnetic saturation values, even when taking magnetically dead layers into account. It was also shown that the simultaneous and pre-introduction methods yielded similar magnetic saturation values despite size differences.

How to cite this article
Hickson MV, Tshentu ZR, Betz R. The Stage Dependent Effect of Capping Agent Introduction in the Synthesis of Magnetite Nanoparticles. Nanochem Res, 2019; 4(2): 119-131. DOI: 10.22036/ncr.2019.02.003

INTRODUCTION

The iron oxide based magnetite nanoparticles are quickly gaining interest in research due to their interesting size related superparamagnetic properties [1]. There are many proposed uses for these nanoparticles such as a hyperthermic agent, waste water treatment, drug delivery, catalyst support, sensor applications, and even information storage [2–4]. For all these purposes the highest quality nanoparticles will be needed. Thus, it is desired to determine the optimal route to obtain the highest quality of magnetite nanoparticles.

The synthesis of magnetite nanoparticles has been well explored through the route of co-precipitation, whereby a precipitating agent such as ammonia is used to precipitate out the nanoparticles from a solution of ferrous and ferric ions under inert conditions [3]. A ratio of 1:2 of ferrous:ferric ions is optimal, yielding particles of highest stability [5]. Higher pH levels result in smaller particles [6]. Exposure to the atmosphere can affect both the size and shape, resulting in the formation of nano-rods as opposed to the desired nano-dots [7]. Lower temperatures lead to the production of smaller magnetite nanoparticles [8]. Lower ionic strengths cause larger particles [9]. Higher stirring speeds of the reaction result in smaller nanoparticles [10].

However, there is still information lacking on how the stage at which the capping agent is introduced affects the quality of the nanoparticles. Nanoparticles require capping agents to be utilized in order to prevent Ostwald ripening from occurring

* Corresponding Author Email: *m.v.hickson@gmail.com*

This work is licensed under the Creative Commons Attribution 4.0 International License.
To view a copy of this license, visit http://creativecommons.org/licenses/by/4.0/.

and are also used to convey desired characteristics to the nanoparticles such as biocompatibility or increasing the ability to become solvated[4, 11]. As such, knowing how the stage at which the capping agent is introduced affects the nanoparticles will be greatly advantageous.

In this study, three different capping methods were applied, being the only allowed variable in the systems. The capping agent was introduced into the system at three different stages; either prior to (Pre-), simultaneously with (Sim-), or post-introduction (Post-) of the precipitating agent. The nanoparticles obtained from these procedures were characterized in terms of TEM, pXRD, EDX, FTIR, XPS, and magnetic analysis to determine which synthetic procedure yielded the highest quality nanoparticles. The experiment was performed using the amino acids L-glutamine (Q) and L-glutamic acid (E) as the capping agents.

EXPERIMENTAL

Chemical and Characterization Details

Iron (II) chloride tetrahydrate (99%) was purchased from Fluka Analytical. Iron (III) Chloride (98 %) and the 25% ammonia solution were provided from Merck. L-glutamine (99%) and L-glutamic acid (99%) were obtained from Sigma. Deionized water from a Millipore Simplicity 185 was used, having a conductivity of 18.2 $M\Omega.cm^{-1}$. TEM and EDX analyses were performed on a JEOL JEM-2100 Electron Microscope operated at 200 keV, with samples placed on holey carbon copper mesh grids. Size determinations were made over at least 1000 particles, measured using ImageJ software. Diffractograms were obtained using a PANalytical XRD Aeris. Samples were run from 10-80° using a Co anode radiation source. Survey scans and high resolution scans were run upon a Cryogen-free ARPES and High-Resolution XPS Apparatus Spectroscopy X-ray Photoelectron Spectroscope. Infrared spectra were determined upon a Bruker Tensor 27 Platinum ATR-FTIR spectrophotometer, at a range of 4000 – 400 cm^{-1}. An average of 32 scans were used, at a resolution of at least 2 cm^{-1}. M-H loops were obtained upon a Quantum Design Inc Squid Magnetometer. Samples were run at room temperature and looped to display reproducibility and coercivity.

The Synthesis of Bare Magnetite Nanoparticles

A 2 mmol (0.3976 g) sample of $FeCl_2.4H_2O$ and 4 mmol (0.6488 g) sample of $FeCl_3$ were dissolved in 50 mL of a 0.2M saline solution made up from Millipore water. The resulting solution was placed under a flowing nitrogen environment and stirred at 600 rpm. Once aptly mixed, the solution was heated to 60°C. To this orange solution, 10 mL of 25% ammonia solution was quickly added resulting in a black precipitate. After stirring for 30 minutes, the particles were magnetically separated and washed with water until pH 7 was obtained. The nanoparticles were then filtered off and dried overnight at 50℃ yielding the bare nanoparticles as a metallic black powder.

The Synthesis of Capped Magnetite Nanoparticles by Pre-Precipitation Introduction of Capping Agent

An 8 mmol (1.1691 g for L-glutamine, 1.1770 g for L-glutamic acid) sample of the appropriate amino acid was suspended in 25 mL of a 0.2 M saline solution, and added to 2 mmol sample of $FeCl_2.4H_2O$ and 4 mmol sample of $FeCl_3$ dissolved in 25 mL of a 0.2M saline solution to obtain a ratio of 1:2:4 of Fe(II):Fe(III):amino acid. The resulting solution was placed under a flowing nitrogen blanket, stirred at 600 rpm and heated to 60°C. Once the desired conditions were reached, 10 mL of 25% ammonia solution was injected quickly into the suspension, resulting in the change of colour from orange to black due to the precipitation of Fe_3O_4 nanoparticles. The suspension was aged for 45 minutes, and the nanoparticles were isolated by means of magnetic separation. The same washing and drying method was applied as per the bare nanoparticles. Overnight drying yielded the capped nanoparticles as a metallic black powder.

The Synthesis of Capped Magnetite Nanoparticles by Simultaneous-Precipitation Introduction of Capping Agent

As per the bare nanoparticles, a 2 mmol sample of $FeCl_2.4H_2O$ and 4 mmol sample of $FeCl_3$ were dissolved in 50 mL of a 0.2M saline solution. The resulting solution was placed under a flowing nitrogen environment, and stirred at 600 rpm, and heated to 60°C. Once the suspension reached the desired temperature, 10 mL of 25% ammonia solution used to dissolve 8 mmol of the appropriate amino acid and was injected quickly into the solution, resulting in the colour change of orange to black. The suspension was aged for 45 minutes, and isolated and dried as per the bare nanoparticles. Overnight drying yielded the capped nanoparticles as a metallic black powder.

The Synthesis of Capped Nanoparticles by Post-Precipitation Introduction of Capping Agent

The procedure described in the synthesis of bare nanoparticles was followed up to the point of neutralization. Following the acquirement of pH 7, the nanoparticles were resuspended in a 0.2 M saline solution containing 8 mmol of the appropriate amino acid. The solution was stirred once again at 600 rpm at 60°C, under a flowing N_2 blanket for 60 minutes. Once completed, the sample was isolated and washed thrice with deionized water *via* the magnetic isolation method. After the final wash, the nanoparticle sample was dried at 50°C to obtain the capped nanoparticles as a metallic black powder.

RESULTS AND DISCUSSION

Transmission Electron Microscopy

Particle distributions were measured over 1000 particles and are displayed parallel to the micrographs. The results are summarized in Table 1 for all seven samples along with their standard deviations and dispersity values. Based on the micrographs of the bare nanoparticles (Fig. 1), a spherical morphology takes precedence with occasional oval and cuboidal shapes occurring. The particle size obtained for the bare nanoparticles was 5.75 ± 2.65 nm, displaying a Gaussian type size distribution. As expected, this reaction resulted in quite a high relative standard deviation of 46.1% due to the lack of constraints put into the reaction to hinder the particle growth.

For the L-glutamine series (Fig. 2) the SimQ sample gave the smallest size of 4.70 ± 1.69 nm, followed by the PreQ sample of 5.12 ± 1.86 nm, while the PostQ sample gave the largest sized nanoparticles of 5.66 ± 1.89 nm. From observing the micrographs, the nanoparticle morphologies of all samples displayed similar spherical shape, with some being cuboidal in nature. Traversing from the PreQ to the SimQ to the PostQ micrographs, a definite decrease in agglomeration is noted. The PreQ samples appears to have agglomerated upon drying, but this decreases significantly moving on to the SimQ sample, and even more so for the PostQ sample. This agglomeration of nanoparticles upon drying is not preventable as it is a symptom of the van der Waals forces, which have a significant effect at the nanometer level [12]. For the relative standard deviations of the L-glutamine series, the value is seen to steadily

Table 1. Nanoparticle sizes as determined by TEM, along with their Dispersity value and crystallite size as determined by XRD.

Particle Type	TEM (nm)	Relative Standard Deviation (%)	Dispersity (Đ)	XRD (nm)
Bare	5.75 (±2.65)	46.09	1.74	7.28
PreQ	5.12 (±1.86)	36.29	1.51	5.09
SimQ	4.70 (±1.69)	35.90	1.45	7.30
PostQ	5.66 (±1.89)	33.42	1.34	8.00
PreE	3.58 (±1.21)	33.79	1.35	5.14
SimE	4.15 (±1.48)	35.71	1.47	5.09
PostE	4.41 (±1.47)	33.22	1.37	7.74

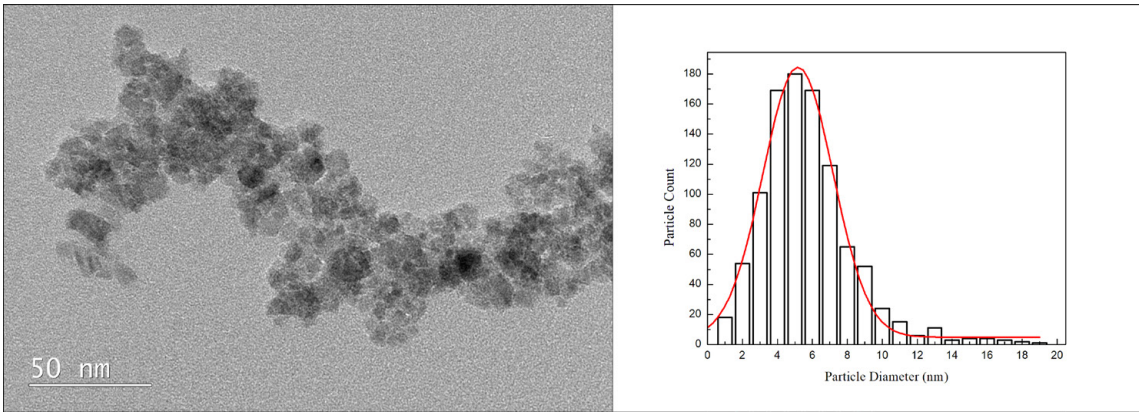

Fig. 1. TEM bright field micrographs of the bare magnetite nanoparticles (left) and the size distribution histogram (right).

CC BY

decrease in the order of PreQ>SimQ>PostQ, with PostQ having the lowest relative standard deviation. Using the L-glutamic acid as a capping agent (Fig. 3), it is seen that the PreE sample yielded the smallest particle size of 3.58 ± 1.21 nm, followed by the SimQ sample of 4.15 ±1.48 nm. The PostE sample once again gave the highest particle size out of the series, 4.41 ± 1.47 nm. Similar to the L-glutamine series, the PreE to SimE to the PostE micrographs display a decrease in agglomeration, as well as relative standard deviations.

Cross examining the methods applied, the small sizes for the pre-addition method are likely to be a result of the coordination ability of amino acids to the iron species. Through this coordination, the capping agents effectively slow down the particle growth, resulting in smaller nanoparticle sizes being obtained[3, 13]. From the simultaneous addition method, seemingly sporadic results are seen. These cannot be rationalized by means of pH change in the simultaneously introduced amino

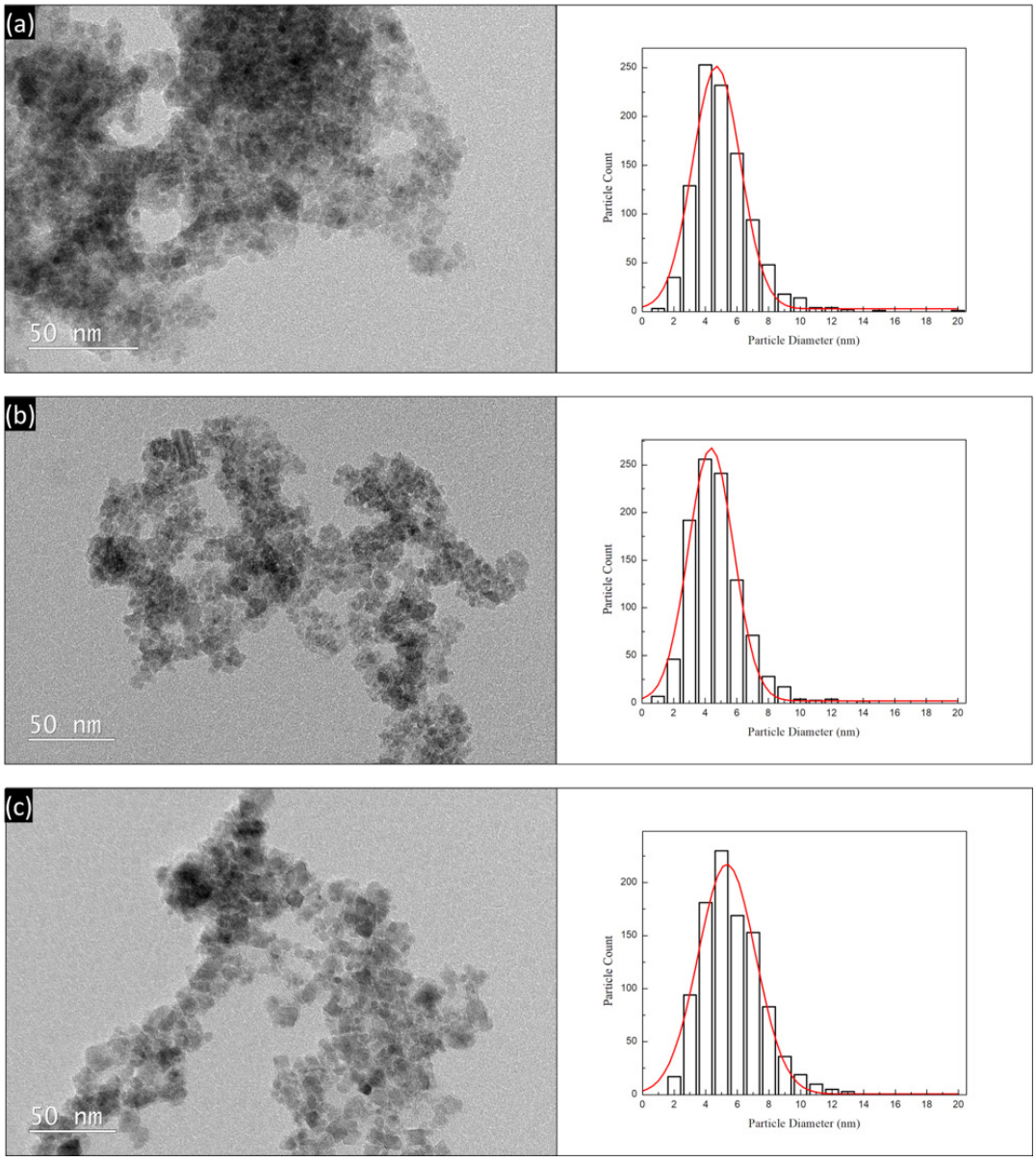

Fig. 2. TEM bright field micrographs (left) and size distribution histograms with Gaussian distributions in red (right) of the L-glutamine series of capped nanoparticles, being PreQ (a), SimQ (b) and PostQ (c).

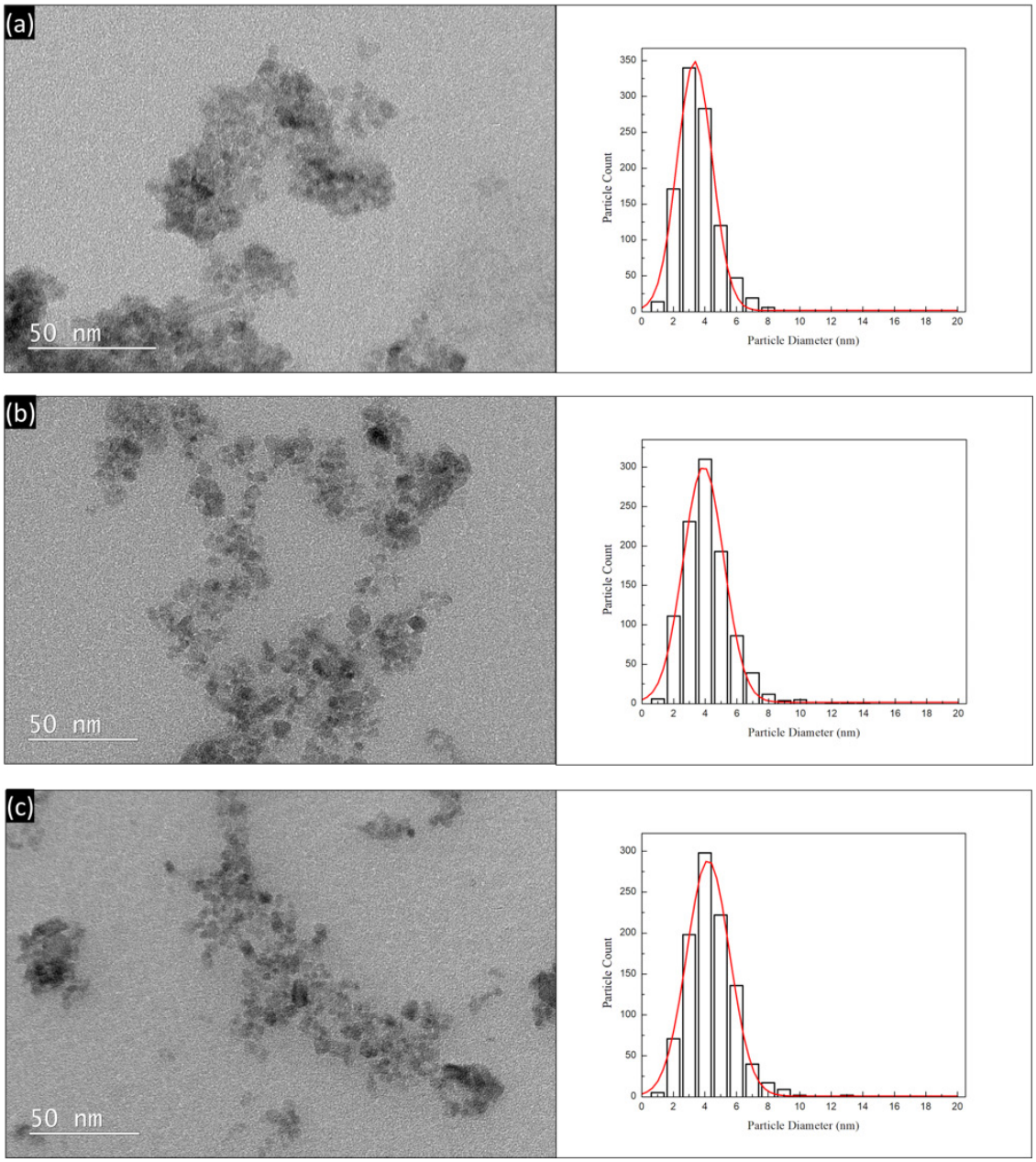

Fig. 3. TEM bright field micrographs (left) and size distribution histograms with Gaussian distributions in red (right) of the L-glutamic acid series of capped nanoparticles, being PreE (a), SimE (b) and PostE (c).

acid and ammonia solution introduced but may be a result of "localized capping" due to their similar sizes. As the ammonia and amino acids are introduced to the solution of Fe(II)/Fe(III) species in the same moment, the instant the nucleation begins the small crystallites are capped and growth is hindered, yielding a particle close to the "time zero" size that experiences negligible growth over time [14]. As SimE is much smaller than SimQ, it is suspected that the increased ability of L-glutamic acid to coordinate through the side chain carboxyl group has such an increased efficiency in preventing growth of the particles.

As expected, the post addition method yielded the largest nanoparticle size out of the applied capping methods. It is of note that the comparison between the bare nanoparticles and the post-capped nanoparticles shows a discrepancy in size,

CC BY

with the capped types being smaller than that of the bare particle type. This difference can be ascribed to the acidity of the amino acids; when dispersed appropriately for the post-capping methodology, the L-glutamic acid suspension pH is 3.22 and the L-glutamine suspension pH is 5.43. As the iron oxide nanoparticles are noted to dissolve in acidic conditions [15], this relative acidity can be accused of etching the upper layers of the nanoparticles before capping and stabilization occurs, resulting in smaller particle sizes. The factor that the L-glutamic acid has both a more acidic pH and a lower particle size gives weight to this theory.

When observing the relative standard deviations of the various methods, the post addition method is consistent for both series in having the lowest value, being the most beneficial to synthesize a sample of nanoparticle that have the lowest relative size distributions. Another apt method of describing the nanoparticles in terms of size distribution is through the dispersity. Dispersity (Đ), formerly known as the polydispersity index, gives an indication of how heterogenous the sizes of nanoparticles in a sample are [16]. A larger dispersity value indicates a higher variation in the size of the nanoparticles in a sample, while a value closer to "1" indicates the nanoparticles are more uniform in size. Naturally, dispersity values are desired to be as close as possible to "1" to have a single size of nanoparticles in the sample being used. Dispersity can be calculated from TEM results using the following formulae:

$$D_n = \frac{\Sigma(d_i)}{n} \quad (1)$$

$$D_w = \frac{\Sigma(d_i)^4}{\Sigma(d_i)^3} \quad (2)$$

$$Đ = \frac{D_w}{D_n} \quad (3)$$

In these formulae, d_i refers to the individual diameters, n is the number of particles, D_n is the mean diameter value, D_w is the weight average diameter, and Đ is the dispersity. These formulae were applied over the 1000 particle measurements as to determine the dispersity of each synthesis type.

Observing these dispersity values for the L-glutamine series, it is noted that a definite decrease in the dispersity is noted of PreQ>SimQ>PostQ, making the size distribution most "homogenous" in nature for the post addition method for the L-glutamine series. Conversely, the dispersity values for the L-glutamic acid syntheses show a vexing notion of the pre-synthesis having a lower dispersity than that of the post-synthesis technique. It is worth noting that the PreE dispersity value is only 0.02 lower than that of PostE but should still be discussed. This discrepancy from what is seen for the L-glutamine series can be accounted for by the small sizes involved in the system. As the PreE synthesis results in nanoparticles smaller in size than PostE, the natural distribution is constrained in terms of how low it can go, thus offsetting the gaussian distribution, and resulting in a slightly lowered dispersity value.

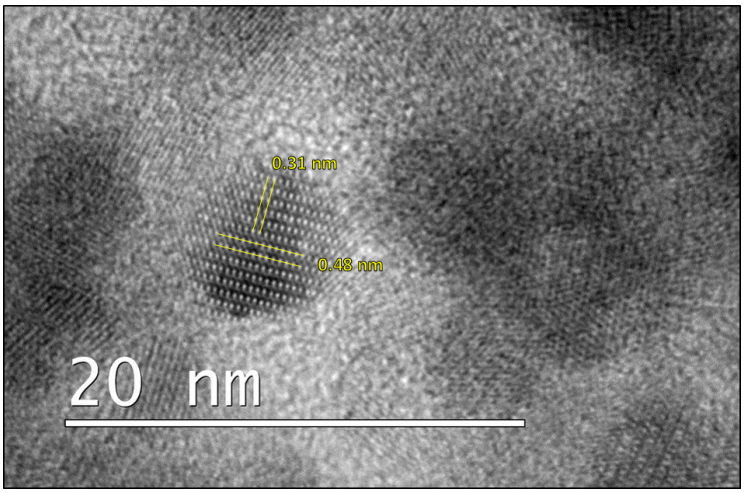

Fig. 4. High resolution TEM micrograph of the SimQ nanoparticle sample, demonstrating the crystallinity of the nanoparticles synthesized.

By using high resolution TEM, the crystal planes of the magnetite nanoparticles can be observed (Fig. 4). Well defined atomic lattice fringes are observable in two directions. The most distinguishable plane of the two has an interplane distance of ~0.48 nm which relates to the (111) crystal plane of magnetite [17]. The second lattice plane has a distance of ~0.31 nm, relating to the (220) crystal plane of magnetite. In conjunction, these show that the synthesis has led to high quality nanoparticles in terms of crystallinity [18].

Powder X-Ray Diffraction Pattern Analysis

To determine crystallite size of the nanoparticles, a powder XRD analysis was performed on the magnetite samples from run from 10 to 80°, using cobalt radiation. The spectra obtained for the L-glutamic series of nanoparticles and the bare nanoparticles can be seen in Fig. 5. The diffractogram of the bare nanoparticles showed several intense reflections, the most prominent of which are the (111), (220), (311), (400), (422), (511), and (440) peaks, confirming the presence of the magnetite phase. Unassigned peaks (*) originate from absorbed NaCl [9]. The lack of peaks which could be ascribed as (104) or (331) displays that other iron oxide phases such as hematite have not been obtained as the major phase [19]. These peaks are present throughout the rest of both the L-glutamine and L-glutamic acid series, displaying that the capping methods did not result in any phase changes and that magnetite nanoparticles are still obtained throughout the various syntheses. However, the peak resolution is seen to vary through the different methods applied.

When comparing the powder spectra of the capped nanoparticles, it is apparent that the highest peak resolution is obtained from the post addition method. This is reflected in the crystallite size determination from the Debye-Scherrer equation, where the most intense peak, namely (311), is used to determine the size of the crystallite:

$$D = \frac{K\lambda}{\beta \cos(\theta)} \quad (4)$$

where D is the diameter of the average crystallite in nm, K is the shape factor, λ is the wavelength of the X-ray applied, β is the mid-peak width of the most intense peak, and θ is the Braggs Angle measured in radians. These results are displayed in Table 1, alongside the TEM results. For the bare nanoparticles, a crystallite size of 7.28 nm is obtained. The pre-addition method yielded smaller crystallites of 5.09 and 5.14 nm respectively for the L-glutamine and L-glutamic acid capping agents, and the simultaneous addition yielded irregular

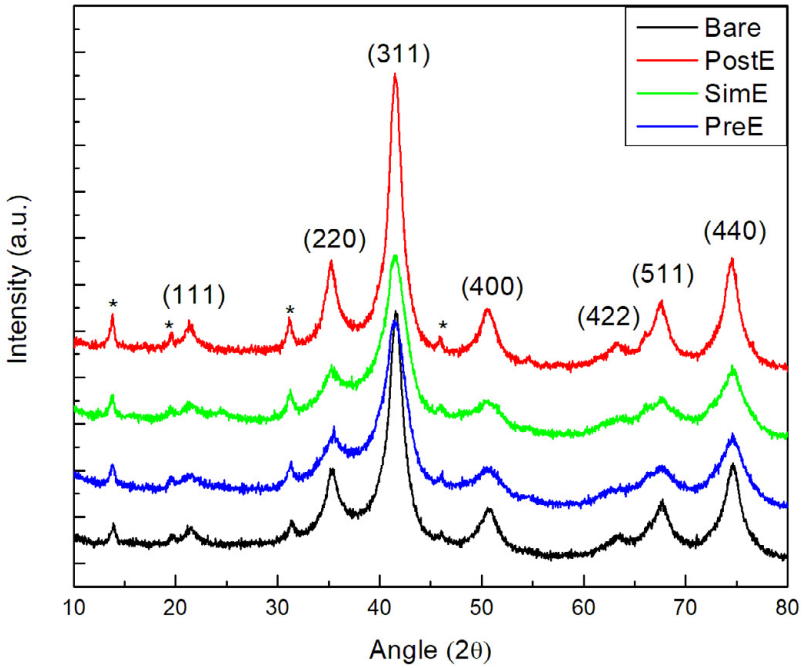

Fig. 5. Powder XRD pattern of the bare nanoparticles, along with the L-glutamic acid series of capped nanoparticles.

CC BY

sizes of 7.30 nm for SimQ and 5.09 nm for SimE. The high resolution TEM displayed the samples as highly crystalline for the SimQ sample, and as such it was expected for this sample to yield such a high crystallite size. For the post addition method, the highest crystallite sizes were obtained, with 8.00 nm for PostQ and 7.74 nm for PostE, exceeding even the value size displayed by the bare nanoparticles. This provides a degree of evidence towards the etching theory of the post addition method discussed in the TEM section. From these factors, it can be taken that the post addition method produces the best crystalline quality, by letting the nanoparticle grow freely and unconstrained, and then removing the upper layers in the capping stage once the growth stage has halted.

Energy Dispersive X-ray Spectroscopy

As to display the elemental make-up of the nanoparticles, EDX spectroscopy was performed upon the samples. Several elemental peaks of note are observed in the spectra (Fig. S1 in Supplementary Material), which are consistently seen throughout the series. The presence of copper, silicon, and carbon peaks seen in the spectra can be accounted for by the holey carbon copper grids used. Peaks originating from the iron and oxygen atoms are observed, indicating that the iron oxide nanoparticles have been synthesized in all cases as expected.

Infrared Spectroscopy

The infrared spectra of magnetite nanoparticles can also give an indication if successful capping has occurred. The most relevant peaks are summarized in Table S1 in Supplementary Material for the bare, L-glutamine and L-glutamic acid capped nanoparticles, and the spectra of the particles can be seen in Fig. 6 for the bare nanoparticles and the L-glutamic acid capped series.

For the bare magnetite nanoparticles, there are three major peaks at 3352, 1634, and 541 cm^{-1}. The peaks at 3352 and 1634 cm^{-1} can be assigned as the stretching and bending modes of (O-H), while the peak at 541 cm^{-1} is that of the (Fe-O) lattice vibrations [20]. The single peak obtained in this region gives a strong indication that the main phase present in the system is magnetite, as other iron oxides such as hematite generally exhibit two or more peaks between 600 to 400 cm^{-1} [21]. The origin of the (O-H) functional groups are from surface edge oxygens existing as hydroxyl groups or from water that has been absorbed onto the surface of the magnetite.

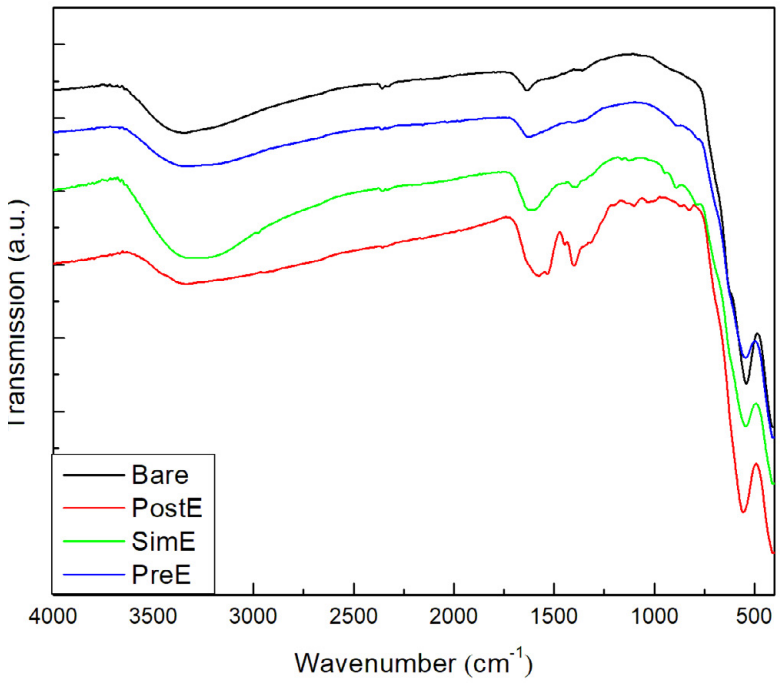

Fig. 6. FT-IR spectra of the bare nanoparticles and the L-glutamic acid series of capped nanoparticles.

For the capped nanoparticles, new peaks are seen to have arisen, relating to the amino acids coating the surface of the nanoparticles. In these, the (Fe-O) vibrations are still plainly visible, along with peaks associated (O-H) vibrations at ~3350 cm^{-1}. Slight shifting of these (O-H) peaks may be associated with overlaid (N-H) vibrations of the amine groups present on the amino acids. Furthermore, in all cases of the capped nanoparticles, a very distinct broadening of the peaks at the ~1630 cm^{-1} areas indicating the successful capping of the nanoparticles. This increase in peak width is a result of the (-COO) groups vibrations overlapping those of the (O-H) and (N-H) vibrations. For the PostE sample, this peak is seen to shift down to 1575 cm^{-1}, a result of strong vibrations of the (N-H) group [22].

The most significant difference between the spectra of the pre-addition, simultaneous addition, and post addition methods is the peak prominence. This is especially apparent for the PostE sample, where the stretches of the side chain (-COO) group are observable at 1534 cm^{-1}.

X-Ray Photoelectron Spectroscopy

XPS can also be used to confirm the successful absorption of the amino acids onto the nanoparticles surface. Initial survey spectra were performed on all the samples to determine which elements were present. Elements found were C, O, and Fe for the uncapped bare nanoparticles, and C, O, N, and Fe for the capped nanoparticles. After confirmation of the presence of elements mentioned, high resolution spectra were obtained. A survey scan can be seen in Fig. 7, and high resolution scans can be seen in Fig. S2 in the Supplementary Material, both obtained from the PostE sample. Peak positions obtained from the spectra are summarized in Tables S2 and S3 in Supplementary Material.

In the high resolution spectra of the region associated with iron, two peaks are observed, the Fe $2p_{3/2}$ and Fe $2p_{1/2}$ peaks. These are seen at ~710 and ~724 eV, respectively, which are characteristic for a sample of magnetite [23, 24]. The broadness of these peaks can be explained by Fe $2p_{3/2}$ and Fe $2p_{1/2}$ signals originating from both the Fe(II) and Fe(III) species, which overlap [25]. It is of note that satellites can be seen in the high resolution spectra of Fe. While this can give an indication that hematite has formed, the peaks are seen to be quite weak, and are well observed in other studies for magnetite. Coupled with the pXRD, FTIR and magnetic studies results give the indication that magnetite is indeed the main phase which has been obtained and that if hematite has formed, it will be due to a small degree of surface oxidation.

The x-ray photoelectron spectra showed the

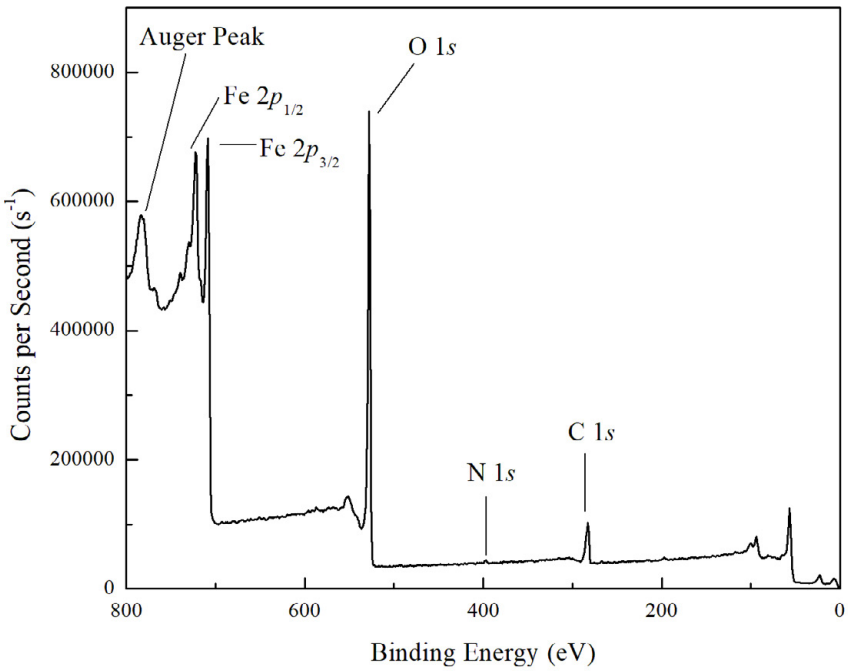

Fig. 7. XPS spectra survey scan of the PostE nanoparticles.

CC BY

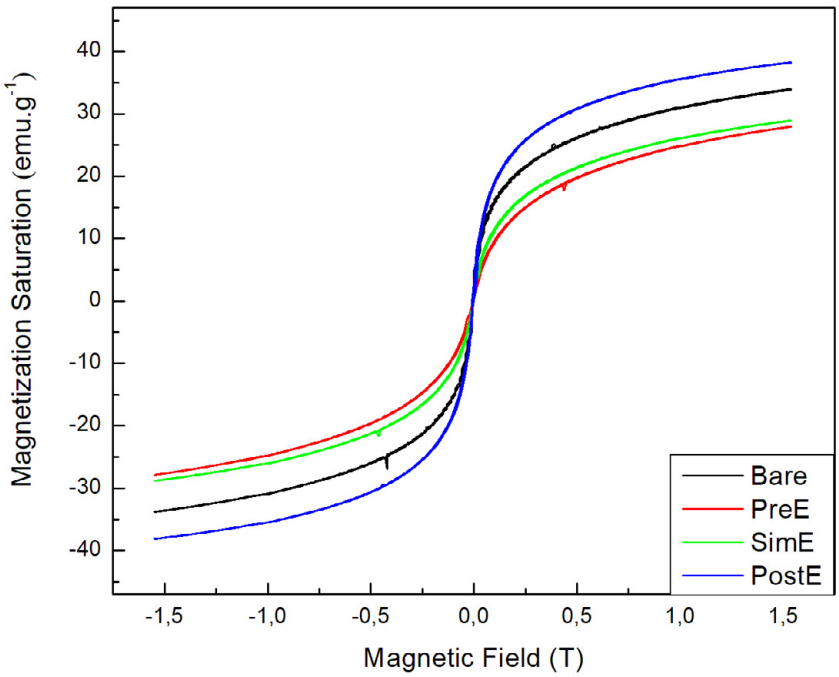

Fig. 8. M-H loops of the bare nanoparticles and the L-glutamic acid series of capped nanoparticles.

presence of carbon on all samples, including that of the bare nanoparticles. This presence of carbon on the bare nanoparticles is noted in literature as originating from the adsorption of carbon dioxide onto the surface of the bare nanoparticle surface [26]. The C 1s peaks seen in the capped nanoparticle series at 283, 285 and 289 eV can be assigned to C-C, C-O, and C=O respectively [27]. It is of note that some spectra displayed only the peaks at 283 or 285 eV in conjunction with the peak at 289 eV.

As stated previously, no nitrogen was found in the scans of the bare magnetite nanoparticles, but the N 1s peak was successfully picked up in the L-glutamine and L-glutamic acid series. This peak appearance confirms the successful capping of the nanoparticles surface with the nitrogen containing organic molecules. The N 1s peak is consistently seen in the 397-400 eV region and can be successfully assigned to C-NH2, the amine group of the amino acids. The asymmetry of this peak can be attributed to hydrogen bonding experienced [21]. The position of the N 1s peaks indicates that no surface interactions take place between the nitrogen and the magnetite surface, as interacting nitrogen shifts up to 402-404 eV, displaying a prominent band [28].

For all samples, oxygen exhibits an O 1s peak around 530 eV. This can be mainly due to the metal oxide, Fe-O [25]. In the high resolution spectra, it is of note that a degree of offset is noted in the peak distribution towards the higher binding energies. This is most likely a result of the extremely intense metal oxide peak overlapping the much less intense C=O and C-O based peaks from the capping agent, which would be at binding energies 3-4 eV higher than the metal oxides.

Magnetic Analysis

The magnetic saturation values for the nanoparticle samples were determined through measuring the magnetization loops at room temperature for each particle type. Magnetization saturation values and the magnetically dead layer sizes determined are seen in Table 2. The M-H loop for the bare and the L-glutamic acid series of capped nanoparticles can be seen in Fig. 8. The difference in magnetizations observed between the samples showed the stage of introduction has a significant effect upon the nanoparticles magnetic properties.

For all samples, the coercivity is seen to be negligible, a characteristic of the superparamagnetic magnetite nanoparticles [6]. When observing the bare nanoparticles magnetic saturation value of 33.27 emu.g^{-1}, it is noted to be vastly below that of bulk magnetite's 92 emu.g^{-1} [29]. As the surface layer has a higher chance of defects, which have a

negative impact on the magnetization saturation, the nanoparticles increase of surface area-to-volume ratio decreases this value substantially [30].

Upon comparison of the magnetic saturation values of the series, it is noted that the pre-addition method consistently gives the lowest saturations of the capped nanoparticles. This may be a result of the complexation between the amino acids and iron ions having a negative impact upon the growth and resultant crystallinity of the obtained nanoparticles, a theorem supported by the XRD results, and thus a lowered magnetic saturation is obtained. It is similarly observed that the simultaneous method did not improve, scarcely increasing the magnetic saturation in either case of L-glutamine or L-glutamic acid from those observed for the pre-addition method. When moving to the post addition methodology, a vast increase in magnetic saturation is displayed compared to the other methodologies. This larger value can be attributed to the higher quality crystallinity obtained from the post addition method, as shown by the XRD results. Upon the introduction and association of the amino acids onto the magnetite surface, the acidity etches off the upper layers of the nanoparticles. As these higher layers have a higher probability of containing the disordered and magnetically inactive layers [30], their removal decreases the degree of crystalline defects resulting in the increase of the magnetic saturation for the post addition type nanoparticles. From these factors, it can be taken that the post-addition methodology creates nanoparticles with the highest quality nanoparticles for magnetic character.

An argument could be made that the magnetic saturation is the highest for the post addition methods merely due to the larger nanoparticles produced, therefore the sizes of the magnetically dead layers must be considered. The size of the dead layer can be calculated from the formula proposed by Safronov, et al:

$$Ms = Ms_{bulk} \cdot \left(1 - \frac{2\Delta}{D}\right)^3 \quad (5)$$

where Ms is the magnetization saturation of the nanoparticle sample, Ms_{bulk} is the magnetization saturation of bulk magnetite, D is the diameter of the nanoparticles, and Δ is the dead layer size [31]. Determined values can be seen in Table 2. This comparison further portrays the efficiency of the post introduction method and is in agreement with the theory of the post addition method etching off the upper layers, by the dead layers of the post addition method being significantly smaller than that of the bare nanoparticles, showing the increase in the ratio of "magnetically active" to "magnetically inactive" sections in the iron oxide nanoparticles crystal system as previously described [6]. As per the results obtained from XPS, this dead layer is most likely to be a hematite phase.

Table 2. The magnetization saturation values and magnetically dead layer size estimation of the nanoparticle samples.

Particle Type	Magnetic saturation ($emu.g^{-1}$)	Dead layer (nm)
Bare	33.27	0.83
PreQ	33.73	0.73
SimQ	33.89	0.67
PostQ	46.50	0.58
PreE	27.59	0.59
SimE	28.92	0.66
PostE	38.24	0.56

When comparing the post addition method to the pre-addition method, a vast improvement is seen for both the L-glutamine and the L-glutamic acid series, having dead layers of 0.58 and 0.56 nm, respectively, of post addition compared to the 0.73 and 0.59 of pre-added. With regards to the simultaneously introduced nanoparticles, sporadic results are once again seen, though in both cases the dead layer values were larger than those of the post addition series. This portrays a less effectual synthesis method, making the simultaneous addition an unviable option. As such, it can be taken that the post addition method yields nanoparticles with the highest quality magnetic properties.

CONCLUSION

In this study, the stage at which the capping agent is added during the synthetic workup was shown to affect the properties of the nanoparticles obtained. The nanoparticles were tested in terms of their size, dispersity, crystallinity, and magnetic character. The successful capping of the nanoparticles was confirmed by both FTIR and X-ray photoelectron spectroscopy. From the TEM results, the post addition resulted in a narrow size distribution, as well as attractive dispersity values. The pre-addition method and simultaneous addition method yielded smaller nanoparticles but with higher relative standard deviations. The crystallite size determined from pXRD showed the post-addition nanoparticles had the highest crystallinity, while the pre-addition and simultaneous-addition nanoparticles were far less crystalline. In terms of magnetic character, the

CC BY

post addition method leads to the highest magnetic saturation value out of the applied techniques. The post addition method also displayed the smallest magnetically dead layer. The simultaneous method was shown to not increase the magnetic saturation value as compared to the pre-addition method despite the size increase. Observing these factors in conjunction, it can be taken that the post-addition methodology produces magnetite nanoparticles of highest quality.

ACKNOWLEDGEMENTS

The authors would like to thank the National Nanoscience Postgraduate Teaching and Training Platform for funding this study. The use of the NEP Physical Properties Measurements on Cryogenic Cryogen free Measurement System at UJ, obtained with the financial support from the SA NRF (Grant No: 88080) and the Faculty of Science, University of Johannesburg (UJ), South Africa, is acknowledged. The use of the Cryogen-free ARPES and High-Resolution XPS Apparatus at the University of Johannesburg (NRF Grant No: 93205) is acknowledged. The assistance by Dr Arno Janse van Vuuren and Ms Candice Blom, Centre for HRTEM, Nelson Mandela University, with the sample analysis on the JEOL JEM-2100 is gratefully acknowledged.

CONFLICT OF INTEREST

The authors declare that there is no conflict of interests regarding the publication of this manuscript.

SUPPLEMENTARY MATERIAL

The Supplementary Material for this article can be found online at: http://nanochemres.org/.

REFERENCES

[1] Mahmoudi M, Sant S, Wang B, Laurent S, Sen T. Superparamagnetic iron oxide nanoparticles (SPIONs): Development, surface modification and applications in chemotherapy. Advanced Drug Delivery Reviews. 2011;63(1-2):24-46.

[2] Gnanaprakash G, Mahadevan S, Jayakumar T, Kalyanasundaram P, Philip J, Raj B. Effect of initial pH and temperature of iron salt solutions on formation of magnetite nanoparticles. Materials Chemistry and Physics. 2007;103(1):168-75.

[3] Laurent S, Forge D, Port M, Roch A, Robic C, Vander Elst L, et al. ChemInform Abstract: Magnetic Iron Oxide Nanoparticles: Synthesis, Stabilization, Vectorization, Physicochemical Characterizations, and Biological Applications. ChemInform. 2008;39(35).

[4] Gupta AK, Gupta M. Synthesis and surface engineering of iron oxide nanoparticles for biomedical applications. Biomaterials. 2005;26(18):3995-4021.

[5] Babes L, Denizot Bt, Tanguy G, Le Jeune JJ, Jallet P. Synthesis of Iron Oxide Nanoparticles Used as MRI Contrast Agents: A Parametric Study. Journal of Colloid and Interface Science. 1999;212(2):474-82.

[6] Kim DK, Zhang Y, Voit W, Rao KV, Muhammed M. Synthesis and characterization of surfactant-coated superparamagnetic monodispersed iron oxide nanoparticles. Journal of Magnetism and Magnetic Materials. 2001;225(1-2):30-6.

[7] Alp E, Aydogan N. A comparative study: Synthesis of superparamagnetic iron oxide nanoparticles in air and N 2 atmosphere. Colloids and Surfaces A: Physicochemical and Engineering Aspects. 2016;510:205-12.

[8] Fang M, Ström V, Olsson RT, Belova L, Rao KV. Particle size and magnetic properties dependence on growth temperature for rapid mixed co-precipitated magnetite nanoparticles. Nanotechnology. 2012;23(14):145601.

[9] Park JY, Patel D, Choi ES, Baek MJ, Chang Y, Kim TJ, et al. Salt effects on the physical properties of magnetite nanoparticles synthesized at different NaCl concentrations. Colloids and Surfaces A: Physicochemical and Engineering Aspects. 2010;367(1-3):41-6.

[10] Mahdavi M, Ahmad M, Haron M, Namvar F, Nadi B, Rahman M, et al. Synthesis, Surface Modification and Characterisation of Biocompatible Magnetic Iron Oxide Nanoparticles for Biomedical Applications. Molecules. 2013;18(7):7533-48.

[11] Yao JH, Elder KR, Guo H, Grant M. Theory and simulation of Ostwald ripening. Physical Review B. 1993;47(21):14110-25.

[12] Wolf EL. Nanophysics and Nanotechnology: John Wiley and Sons; 2008.

[13] Wang Z, Zhu H, Wang X, Yang F, Yang X. One-pot green synthesis of biocompatible arginine-stabilized magnetic nanoparticles. Nanotechnology. 2009;20(46):465606.

[14] Si S, Li C, Wang X, Yu D, Peng Q, Li Y. Magnetic Monodisperse Fe3O4Nanoparticles. Crystal Growth & Design. 2005;5(2):391-3.

[15] Baumgartner E, Blesa MA, Marinovich HA, Maroto AJG. ChemInform Abstract: Heterogeneous electron transfer as a pathway in the dissolution of magnetite in oxalic acid solutions. Chemischer Informationsdienst. 1983;14(45).

[16] Nematollahzadeh A, Abdekhodaie MJ, Shojaei A. Submicron nanoporous polyacrylamide beads with tunable size for verapamil imprinting. Journal of Applied Polymer Science. 2011;125(1):189-99.

[17] Iyengar SJ, Joy M, Maity T, Chakraborty J, Kotnala RK, Ghosh S. Colloidal properties of water dispersible magnetite nanoparticles by photon correlation spectroscopy. RSC Advances. 2016;6(17):14393-402.

[18] Sun S, Zeng H. Size-Controlled Synthesis of Magnetite Nanoparticles. Journal of the American Chemical Society. 2002;124(28):8204-5.

[19] Radu T, Iacovita C, Benea D, Turcu R. X-Ray Photoelectron Spectroscopic Characterization of Iron Oxide Nanoparticles. Applied Surface Science. 2017;405:337-43.

[20] Cornell RM, Schwertmann U. The iron oxides: structure, properties, reactions, occurrences and uses: John Wiley & Sons; 2003.

[21] Krehula S, Musić S. The influence of Cd-dopant on the properties of α-FeOOH and α-Fe2O3 particles precipitated

CC BY

in highly alkaline media. Journal of Alloys and Compounds. 2007;431(1-2):56-64.
[22] Schwaminger SP, García PF, Merck GK, Bodensteiner FA, Heissler S, Günther S, et al. Nature of Interactions of Amino Acids with Bare Magnetite Nanoparticles. The Journal of Physical Chemistry C. 2015;119(40):23032-41.
[23] Yu BY, Kwak S-Y. Assembly of magnetite nanocrystals into spherical mesoporous aggregates with a 3-D wormhole-like pore structure. Journal of Materials Chemistry. 2010;20(38):8320.
[24] Zhao H, Chen Z, Tao L, Zhu X, Lan M, Li Z. In vitro toxicity evaluation of ultra-small MFe2O4 (M = Fe, Mn, Co) nanoparticles using A549 cells. RSC Advances. 2015;5(84):68454-60.
[25] Lai Y, Yin W, Liu J, Xi R, Zhan J. One-Pot Green Synthesis and Bioapplication of l-Arginine-Capped Superparamagnetic Fe3O4 Nanoparticles. Nanoscale Research Letters. 2009;5(2):302-7.
[26] Pavelec J, Hulva J, Halwidl D, Bliem R, Gamba O, Jakub Z, et al. A multi-technique study of CO2 adsorption on Fe3O4 magnetite. The Journal of Chemical Physics. 2017;146(1):014701.
[27] Moulder JF, Stickle WF, Sobol PE, Bomben KD. Handbook of X-ray Photoelectron Spectroscopy; Chastain, J. Perkin-Elmer Corp, Eden Prairie, MN. 1992.
[28] Ataman E, Isvoranu C, Knudsen J, Schulte K, Andersen JN, Schnadt J. Adsorption of L-cysteine on rutile TiO2(110). Surface Science. 2011;605(1-2):179-86.
[29] Landfester K, Ram rez LP. Encapsulated magnetite particles for biomedical application. Journal of Physics: Condensed Matter. 2003;15(15):S1345-S61.
[30] Kaiser R, Miskolczy G. Magnetic Properties of Stable Dispersions of Subdomain Magnetite Particles. Journal of Applied Physics. 1970;41(3):1064-72.
[31] Safronov AP, Beketov IV, Komogortsev SV, Kurlyandskaya GV, Medvedev AI, Leiman DV, et al. Spherical magnetic nanoparticles fabricated by laser target evaporation. AIP Advances. 2013;3(5):052135.

CC BY